Supplemental Information

Src activation by β-adrenoreceptors is a key switch for tumour metastasis

Guillermo N. Armaiz-Pena, Julie K. Allen, Anthony Cruz, Rebecca L. Stone, Alpa M. Nick, Yvonne G. Lin, Liz Y. Han, Lingegowda S. Mangala, Gabriel J. Villares, Pablo Vivas-Mejia, Cristian Rodriguez-Aguayo, Archana S. Nagaraja, Kshipra M. Gharpure, Zheng Wu, Robert D. English, Kizhake V. Soman, Mian M.K. Shazhad, Maya Zigler, Michael T. Deavers, Alexander Zien, Theodoros G. Soldatos, David B. Jackson, John E. Wiktorowicz, Madeline Torres-Lugo, Tom Young, Koen De Geest, Gary E. Gallick, Menashe Bar-Eli, Gabriel Lopez-Berestein, Steve W. Cole, Gustavo E. Lopez, Susan K. Lutgendorf and Anil K. Sood

Supplementary Figure 1

a

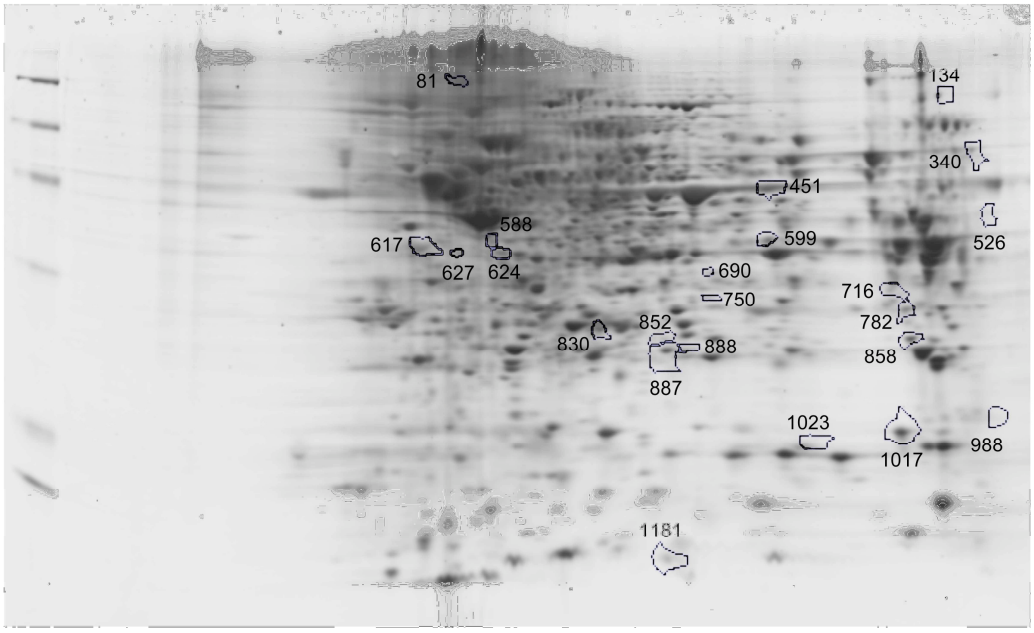

b

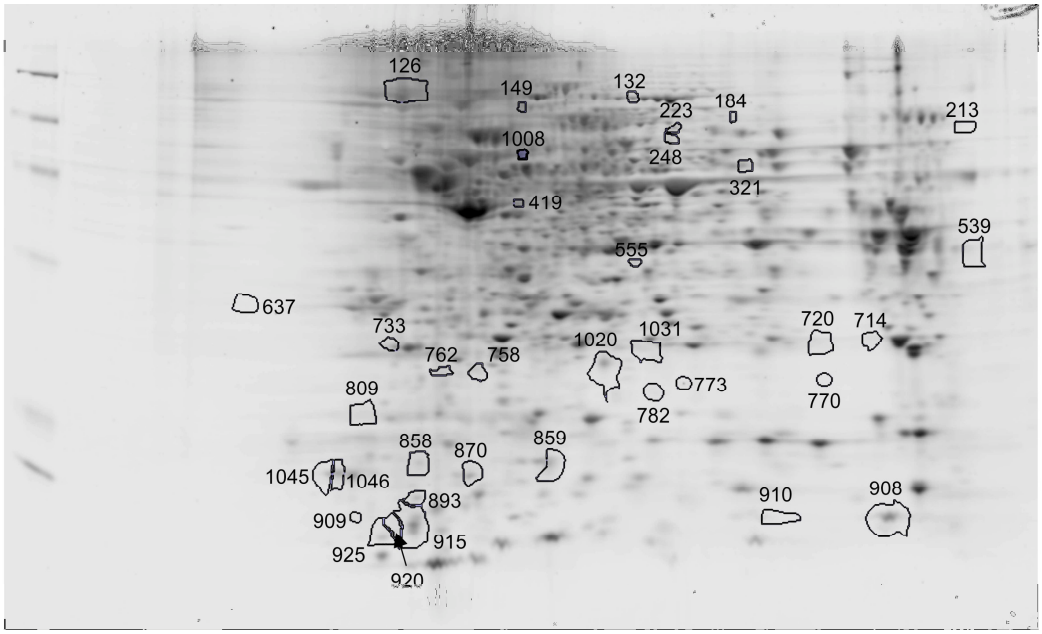

Supplementary Figure 1. Separation of total and phosphorylated proteins by two-dimensional gel electrophoresis. Three sets of samples – Control, 15 minute, and 30

minute – in technical duplicate, were stained with ProQ Diamond followed by Sypro Ruby, to determine phosphorylation and total protein abundance respectively, and imaged. These two sets of six images were then analyzed, separately, using SameSpots v4.1 (Nonlinear Dynamics, Newcastle Upon Tyne, UK). A reference gel was selected by the program and all other images were aligned to it. Spot volume normalization with respect to the reference gel was performed. Spots in the 15 Min and 30 Min samples were quantitatively compared to those in the Control, separately within the Sypro Ruby- and ProQ Diamond- stained groups, to determine differential protein abundance and phosphorylation, respectively. Fold-changes were calculated as ratios of average normalized spot-volumes, and statistical p-values by t-tests. Spots with $P \leq 0.05$ were taken to represent differential phosphorylation/abundance. Proteins identified by mass spectrometry are shown in this figure: **(a)** Proteins showing differential abundance (fold change >1.5 up or down and $P < 0.05$) as determined from the analysis of Control, 15 Min and 30 Min gels stained with Sypro Ruby. The reference gel is shown, with the 23 spots outlined and numbered. Note that the contiguous spots 887 and 888 along a horizontal line, have both been identified as peroxiredoxin-1 (see Supplementary Table 1) suggesting they are post-translational modifications that affect the pI, but not the Molecular Weight. **(b)** Proteins showing differential phosphorylation (fold change >1.5 up or down and $P < 0.05$) as judged from the analysis of control, 15 Min and 30 Min gels stained with ProQ Diamond. The reference gel is shown, with the 36 spots outlined and numbered.

Supplementary Figure 2

a

Kinase	Score
SRC	37 (20)
PRKCA	36 (20)
INSR	33 (18)
IGF1R	33 (18)
CDK2	17 (9)
CK2A1	17 (8)
CSNK2A2	17 (8)
EPHA4	15 (9)
EPHA7	15 (9)
EPHA3	15 (9)
MAP2K4	14 (9)
MAP2K6	13 (7)
MAP2K3	13 (7)
ATM	13 (8)
LCK	13 (9)
ABL1	11 (7)
LYN	11 (8)
DMPK	10 (5)
CSF1R	9 (6)
ENSP00000314228	9 (5)

b

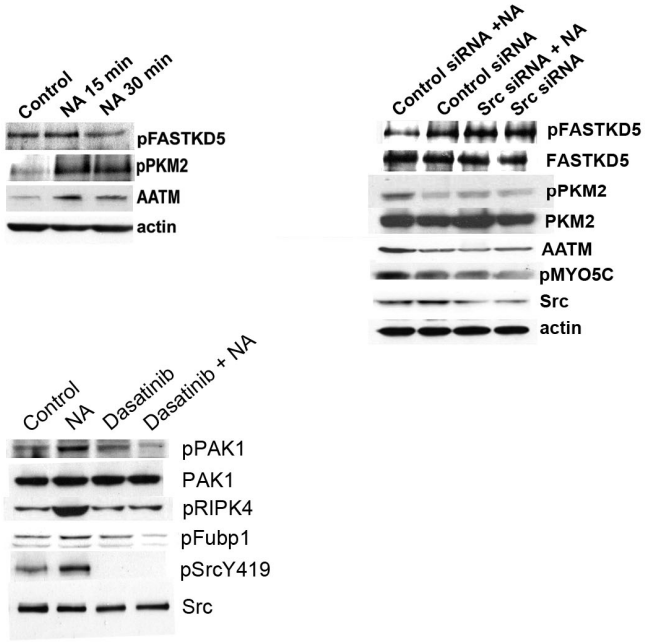

Supplementary Figure 2. Src is key regulator of NA-induced signaling networks. **(a)** Kinase scoring resulting from the construction of a two-layer phosphorylation network upstream of identified proteins using data from Phospho.ELM and networKIN. The numbers in parentheses are the corresponding scores restricted to the differentially phosphorylated proteins. (**b)** Validation of selected proteins identified as differentially phosphorylated or expressed by proteomics analysis. SKOV3ip1 cells were treated with 10 μM NA for 15 and 30 min. Cell lysate was collected and subjected to Western blot analysis. In separate experiments, SKOV3ip1 cells were pre-treated with either Src siRNA or dasatinib. Cells were then treated with 10 μM NA for 30 min and their lysate collected and subjected to Western blot analysis.

Supplementary Figure 3

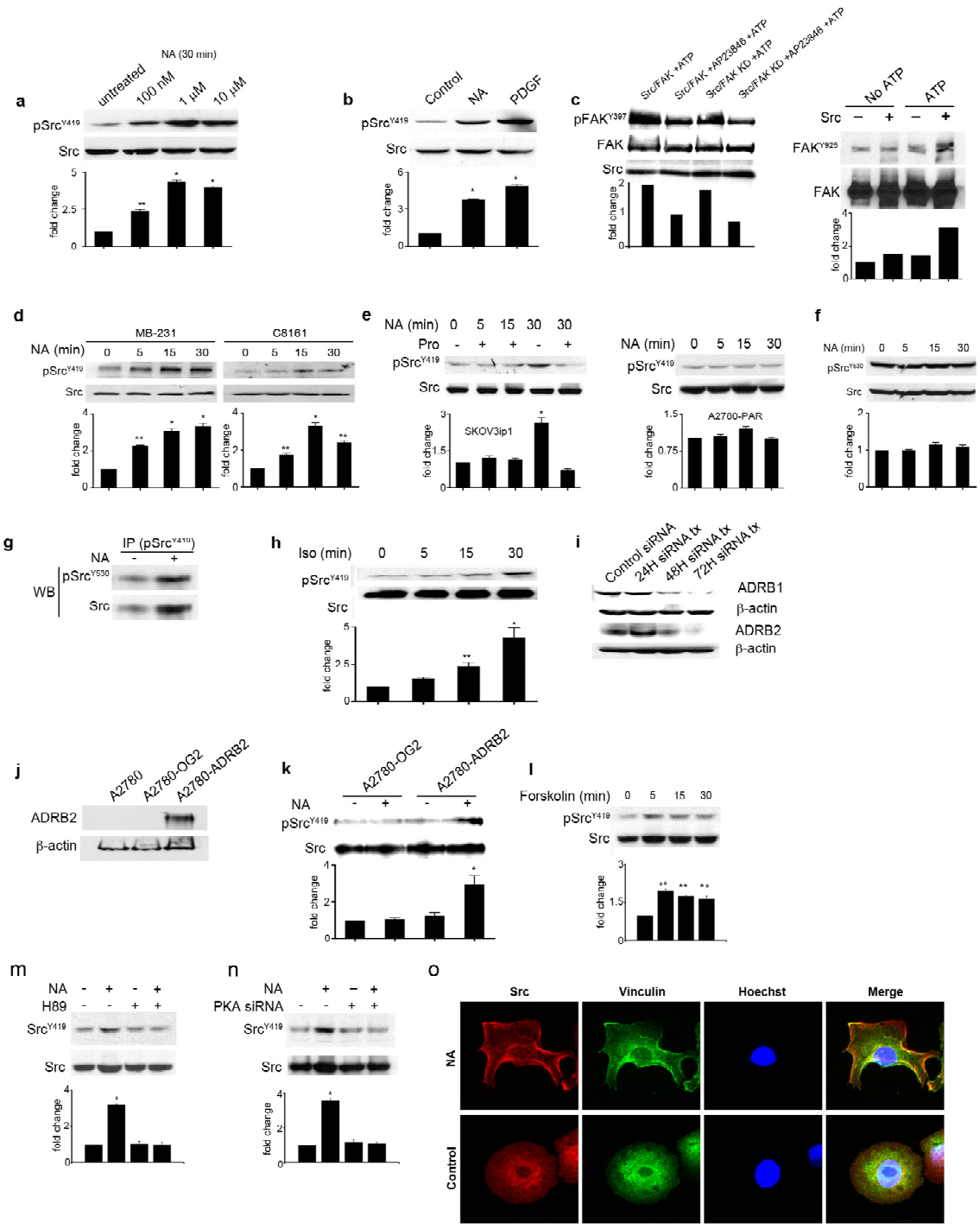

Supplementary Figure 3. An ADRB/cAMP/PKA axis mediates NA-induced Src activation. (a) SKOV3ip1 cells were treated for 30 min with increasing concentrations of NA. Their lysate collected, and subjected to Western blot analysis. **(b)** SKOV3ip1 cells were treated with platelet-derived growth factor BB (PDGF; 20ng/mL) or 10 μM NA for 30 mins. Afterwards, their lysate was analyzed by Western blot. **(c)** Src phosphorylates FAK or kinase dead FAK at Y397 and Y925 (i.e., mutation at K454M, resulting in alteration of the ATP-binding site) as shown by kinase assay analysis. The kinase reaction was carried out by adding kinase buffer containing no ATP, ATP and/or AP23846 and incubating for 30 minutes. The reaction was stopped and samples subjected to Western blot analysis. **(d)** ADRB-positive breast (MD-231) and melanoma (C8161) cells were exposed to 10 μM NA. After treatment, lysates were collected and subjected to Western blot analysis. **(e)** ADRB-null A2780-PAR cells were exposed to 10 μM NA for up to 30 min, their lysate collected and subjected to Western blot analysis. SKOV3ip1 cells were incubated with 1 μM propranolol for 1 h before being treated with 10 μM NA. Lysates were collected and subjected to Western blot analysis. **(f-g)** SKOV3ip1 cells were treated with 10 μM NA for 30 min. After treatment, lysates were collected and subjected to either Western blot analysis for $pSrc^{Y530}$ or immnunoprecipitated with a $pSrc^{Y419}$/Agarose A complex and probed by Western blot analysis for $pSrc^{Y530}$. **(h)** SKOV3ip1 cells were treated with 10 μM isoproterenol, their lysate collected and analyzed by Western blot. **(i)** *in vitro* knockdown of ADRB1 and ADRB2 by targeted siRNA in SKOV3ip1 cells. **(j)** Expression of ADRB2 in A2780-PAR cells stably transduced with either empty (OG2) or ADRB2 expression vector. **(k)** A2780-PAR cells transduced with either OG2 or ADRB2 were exposed to 10 μM NA for

30 min. Their lysates were collected and subjected to Western blot analysis for $pSrc^{Y419}$. **(l)** SKOV3ip1 cells were treated with 1 μM forskolin for up to 30 min. Their lysates were collected and analyzed for $pSrc^{Y419}$ by Western blot. **(m)** SKOV3ip1 cells were incubated with H89 (PKA inhibitor) for 1 hr and stimulated with 10 μM NA, and probed for pSrcY419. **(n)** Similar experiments were performed with siRNA targeted against PKA in SKOV3ip1 cells. **(o)** SKOV3ip1 cells were treated with 10 μM NA, and Src was visualized by immunofluorescence. ** $P < 0.01$; two-tailed t-test; * $P < 0.001$; two-tailed t-test.

Supplementary Figure 4

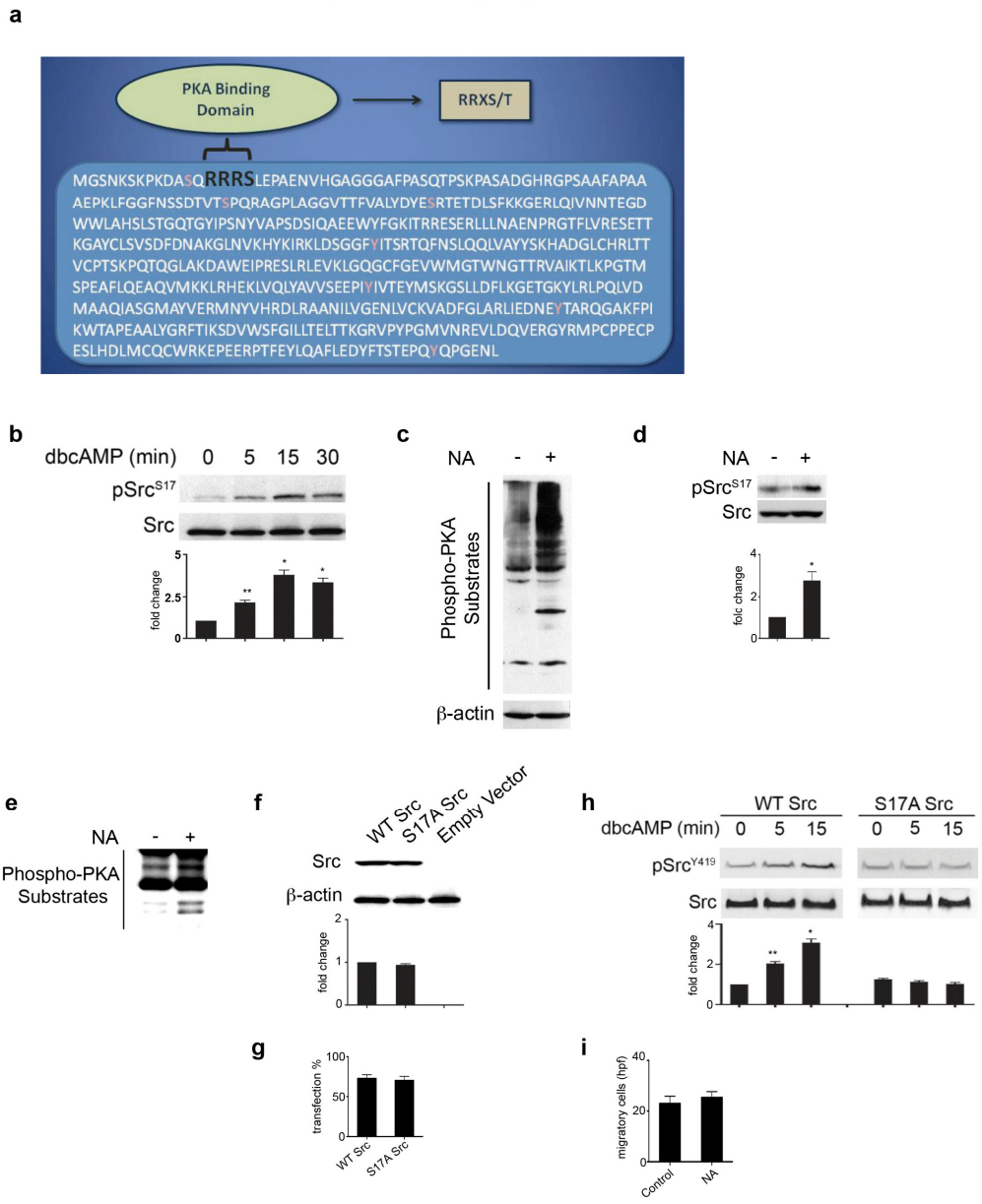

Supplementary Figure 4. PKA directly phosphorylates Src at S17. (a) Src amino acid sequence highlighting the PKA consensus site. **(b)** SKOV3ip1 cells were treated with 50 μM dbcAMP for up to 30 min. Lysates were collected and subjected to Western blot analysis for $pSrc^{S17}$. A2780-ADRB2 cells were treated with 10 μM NA for 30 min

and probed for **(c)** phospho-PKA substrates and **(d)** $pSrc^{S17}$ by Western blot analysis. **(e)** SYF cells were treated with 10 μM NA for 15 min. Their lysates were collected and analyzed for phospho-PKA substrates by Western blot analysis. **(f)** SYF cells were transfected with plasmids containing either wild-type Src (WT Src) or Src mutated at S17 (S17A Src). After transfection, lysates were collected and probed for Src expression by Western blot. **(g)** The transfection efficiency of WT Src or S17A Src plasmids was measured by determining the percentage of Flag-positive cells after immunofluorescence staining. **(h)** SYF cells were transfected with WT Src or S17A Src and exposed to 50 μM dbcAMP. Lysates were collected and analyzed for $pSrc^{Y419}$ by Western blot. **(i)** 10 μM NA did not increase migration of non-transfected SYF cells. ** $P < 0.01$; two-tailed t-test; * $P < 0.001$; two-tailed t-test.

Supplementary Figure 5

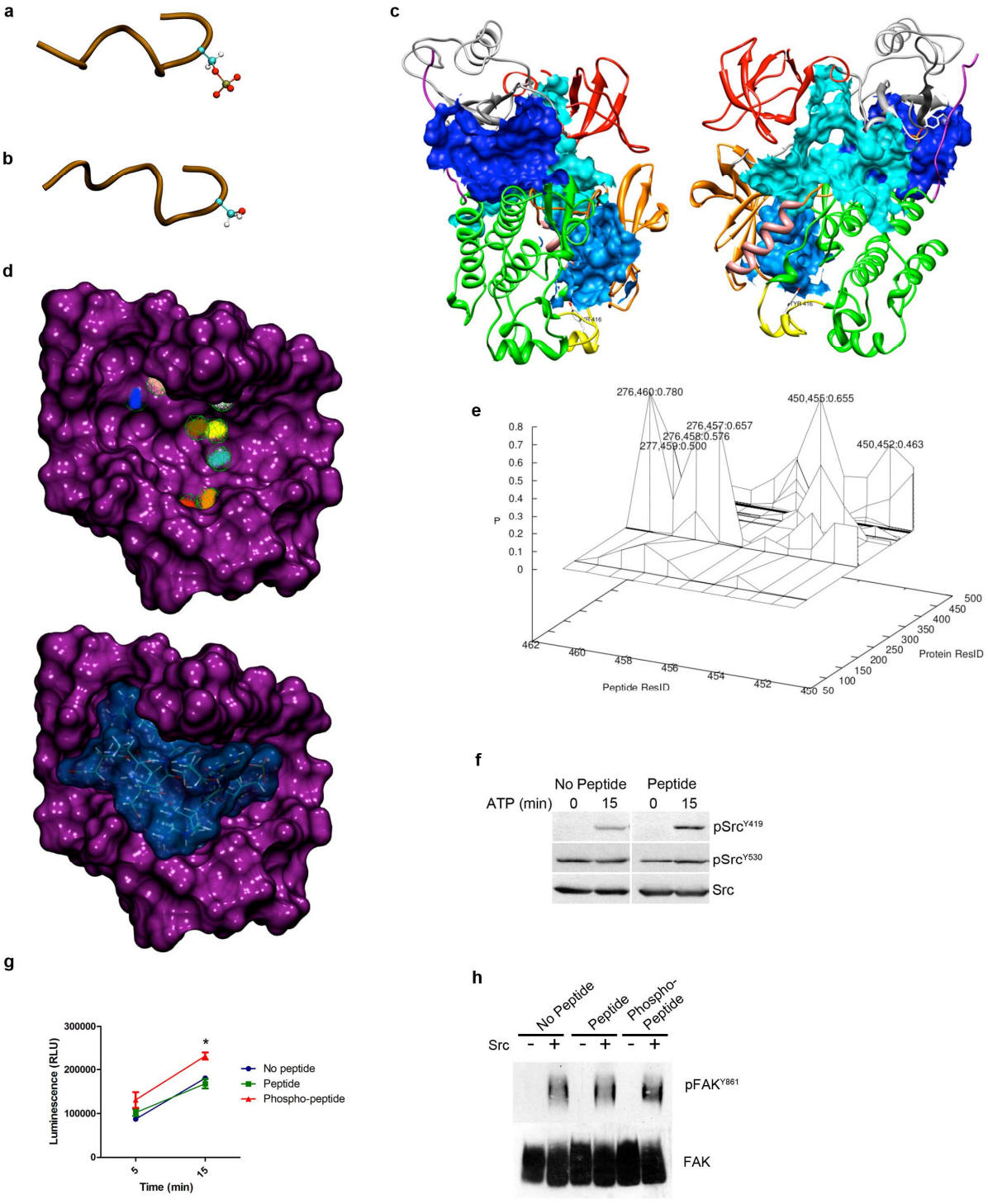

Supplementary Figure 5. pSrc^{S17} can interact with a highly negative cavity between the SH2 and kinase domains near the C-terminus inducing Src activation. Structures of the generated model peptides that resemble the K9-E19 segment of Src in **a)** phosphorylated, and **b)** unphosphorylated forms. **(c)** Two additional views of the three identified cavities where the peptide could be inserted. **(d)** The proposed allosteric binding site of the Src peptide inhibitor. Eight thermodynamically unfavorable hydration sites (shown in green wireframes) were identified. The upper model shows the water density in each of these sites as shown by the variously colored dots. The lower model represents the docked peptide, which displaces water from each of these sites. The displacement of water from these unstable regions should have a favorable contribution to the affinity of the peptide binding at this site. **(e)** Contact probability at a residue function in the peptide and protein residue. The protein residues have been numbered from 1 to 430, and the residues in the peptide from 430 to 462. The numbers depicted on the various peaks have indexes of: Protein Residue ID, Peptide Residue ID: Probability of contact. For example the peak corresponding to 276, 460; 0.78 implies that residue 276 (protein) is in contact with residue 460 (peptide) 78% of the total simulation time. **(f)** A small peptide (phosphorylated at S17 that includes residues K9 to E19 of Src) induces Src phosphorylation at Y419 as shown by kinase assay analysis. The kinase reaction was carried out by adding kinase buffer containing ATP and the pS17 peptide and incubating for 15 minutes. The reaction was stopped and samples were subjected to Western blot analysis. **(g)** A small peptide (phosphorylated at S17 that includes residues K9 to E19 of Src) induces Src enzymatic activity as demonstrated by increased ADP formation (ADP-

Glo Kinase Assay; Promega). In contrast, addition of the same peptide, but unphoshphorylated at S17 did not affect Src activity. **(h)** A small peptide (phosphorylated at S17 that includes residues K9 to E19 of Src) induces Src-dependent phosphorylation of FAK at Y861 as shown by kinase assay analysis. The kinase reaction was carried out by adding kinase buffer containing ATP, the pS17 or unphosphorylated peptide and incubating for 15 minutes. The reaction was stopped and samples were subjected to Western blot analysis. * $P < 0.01$; two-tailed t-test.

Supplementary Figure 6

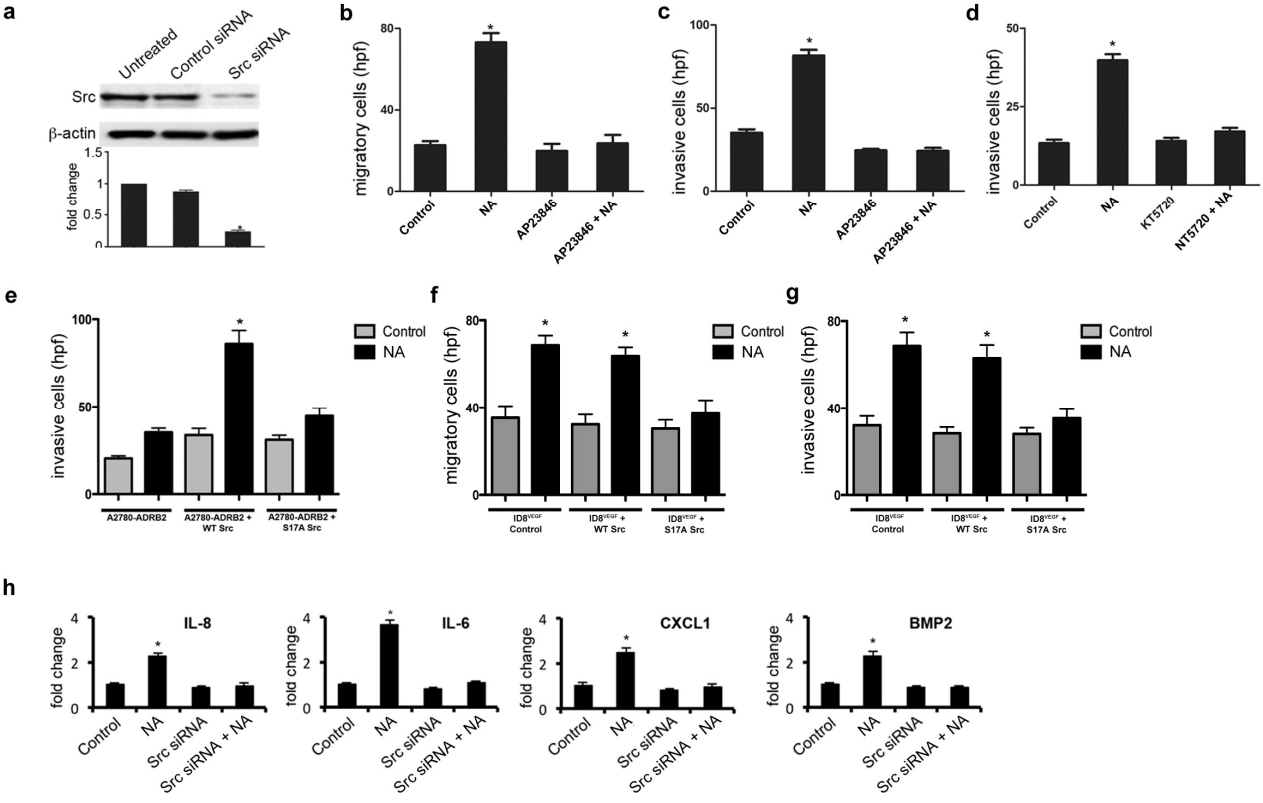

Supplementary Figure 6. Increased adrenergic signaling leads to Src activation, increased cell migration and invasion. (a) SKOV3ip1 cells were transfected for 48 h with Src siRNA. Lysates were collected and analyzed for Src protein levels by Western blot. **(b)** 10 μM NA increased the migratory ability of SKOV3ip1 cells, meanwhile 10 μM AP23846 completely abrogated this effect. SKOV3ip1 cells were subjected to invasion assays. 10 μM NA induced cellular invasion that was completely abrogated by **(c)** 10 μM AP23846 and **(d)** 10 μM KT5720. **(e)** A2780-ADRB2 cells were transiently transfected with either WT or mutant Src (S17A) and stimulated with 10 μM NA and subjected to an invasion assay. Murine ovarian carcinoma cells ($ID8^{VEGF}$) where

transfected with either human WT or mutant Src (S17A), treated with siRNA targeted against murine Src and stimulated with 10 μM NA and subjected to **(f)** migration or **(g)** invasion assays. **(h)** cDNA analysis identified IL8, IL-6, CXCL1 and BMP2 as genes upregulated by NE treatment in SKOV3ip1 cells. This effect was completely abrogated by Src siRNA treatment.

Supplementary Figure 7

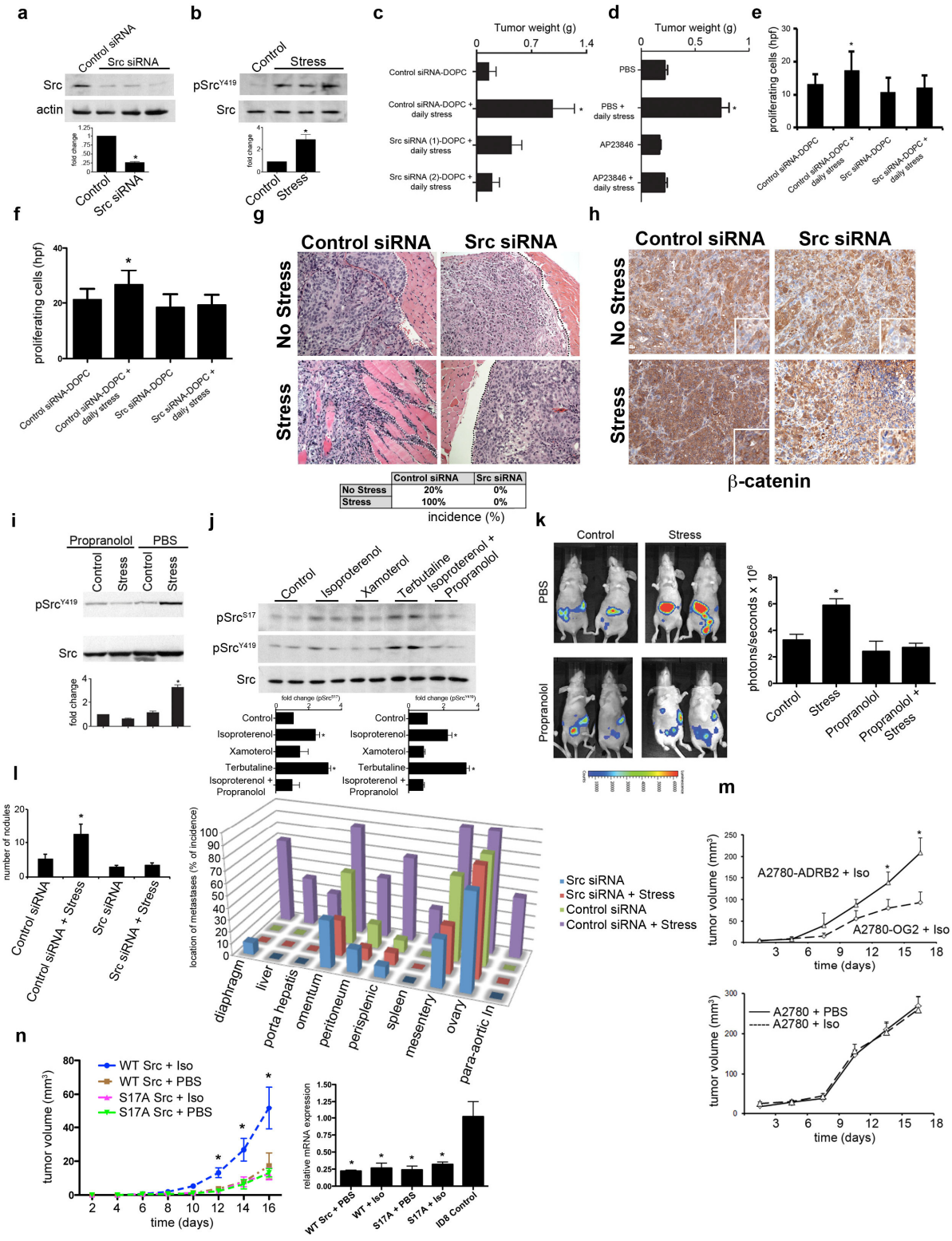

Supplementary Figure 7. Increased adrenergic signaling leads to *in vivo* Src activation, increased invasion and tumour growth. (a) Tumour bearing mice (SKOV3ip1 orthotopic model) were subjected to daily restraint stress for one week, sacrificed and tumours harvested and prepared for Western blot analysis of $pSrc^{Y419}$. **(b)** Western blot of lysate from orthotopic tumours collected 48 hours after a single administration of control siRNA-DOPC or Src siRNA-DOPC. **(c)** Effect of control siRNA-DOPC or two different Src siRNA-DOPC nanoliposomes on restraint-stress induced tumour growth in the SKOV3ip1 model. **(d)** Effect of AP23846 (50 mg/kg) on restraint-stress induced tumour growth in the SKOV3ip1 model. Tumour tissues from daily restraint mice that were treated with control siRNA-DOPC or Src siRNA-DOPC were analyzed by IHC for the proliferation markers **(e)** phospho-histone 3 and **(f)** PCNA. Graph shows phospho-histone 3 or PCNA-positive cells per hpf (20X; * $P < 0.01$; unpaired student t-test). Sections were obtained from tumour bearing mice subjected to daily restraint and treated with control siRNA-DOPC or Src siRNA-DOPC. These sections were stained with **(g)** H&E or analyzed for **(h)** β-catenin expression. **(i)** Tumour lysates from mice exposed to daily restraint and treated with propranolol were subjected to Western blot analysis and probed for $pSrc^{Y419}$. **(j)** HeyA8 tumour lysates from mice treated with either isoproterenol (10 mg/kg), xamoterol (1 mg/kg), terbutaline (5 mg/kg) or isoproterenol (10 mg/kg)/propranolol (2 mg/kg) were analyzed by Western blot for $pSrc^{Y419}$ and $pSrc^{S17}$. **(k)** Noninvasive imaging of metastasis and tumour growth *in vivo*. Luciferase-expressing SKOV3ip1 cells were injected to mice. After injection mice were separated into four groups: No stress/PBS, stress/PBS, no stress/propranolol or stress/propranolol. Mice were then imaged 3 weeks later to assess tumour growth and

metastasis. Representative images are shown. **(l)** Effect of daily restraint stress on metastatic patterns. SKOV3ip1 cells were injected directly into the mouse ovary through a surgical skin incision. One week later, nude mice were subjected to daily restraint stress for 4 weeks and treated with either Src siRNA-DOPC or Control siRNA-DOPC twice a week. At the end of the study, mice were sacrificed, and tumours were harvested. Average number tumour of nodules and percent of animals in each study arm with metastasis to intraperitoneal and distant organ sites are shown. Para-aortic lymph nodes are depicted as *para-aortic LN*. **(m)** Mice were injected s.c. with A2780-PAR, A2780-OG2 (Empty Vector) or A2780-ADRB2 (ADRB2-expressing) cells, and treated daily with isoproterenol (10 mg/kg) or PBS. Tumours were measured every three days and tumour volumes were calculated as (length / 2) x ($width^2$). **(n)** Mice were injected s.c. with murine $ID8^{VEGF}$ ovarian carcinoma cells that were transfected with human WT or Mutant (S17A) Src and treated daily with isoproterenol (10mg/kg) or PBS. Starting two days after tumour cell inoculation, mice were administered murine Src siRNA-DOPC twice a week. Tumours were measured every three days and tumour volumes were calculated as (length / 2) x ($width^2$). Murine Src mRNA levels were determined by real time RT-PCR in each group. Average fold change in murine Src mRNA is reported. * $P < 0.01$.

Supplementary Figure 8

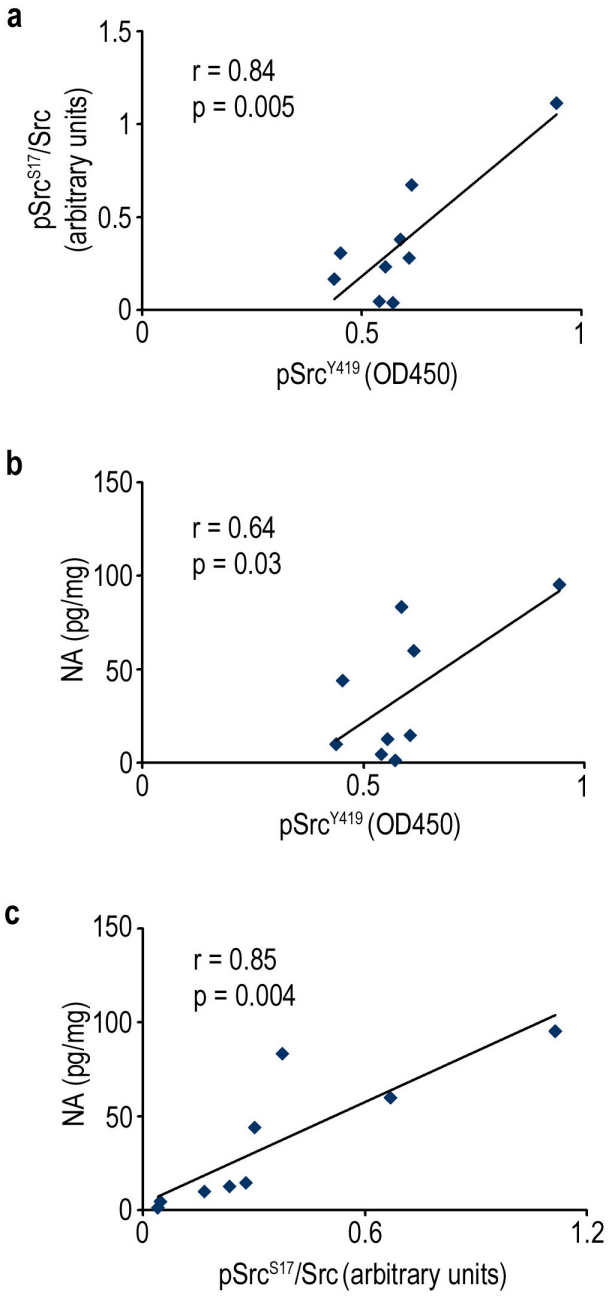

Supplementary Figure 8. Increased pSrc^{S17} and pSrc^{Y419} correlates with increased intratumoural NA. A subset of patient samples was analyzed for pSrc^{S17} and pSrc^{Y419} levels by Western blot and ELISA, respectively. **(a)** Regression analysis shows that Src^{S17} phosphorylation correlates with Src^{Y419} phosphorylation. Moreover, there was a strong correlation of **(b)** pSrc^{Y419} and **(c)** pSrc^{S17} with intratumoural NA. The Spearman correlation coefficient was calculated for each correlation.

Supplementary Table 1

	Protein name[a]	Swissprot accession	Gel spot No[b].	pI[c]	MW (kD)[c]	MS ID Expecta-tion value[d]	Peptide count[e]	Un-matched masses[f]	Sequence coverage[g] (%)	Relative protein abundance[h]		T-test p-value[h]	
										15 Min	30 Min	15 Min	30 Min
1	Transitional endoplasmic reticulum ATPase - Homo	TERA_HUMAN	81	5.57	119.031	6.29E-32	20	7	24	-1.36	-1.77	0.1391	0.0403
2	Serpin H1 precursor - Homo sapiens (Human)	SERPH_HUMAN	134	8.78	102.495	5.00E-10	6	9	16	-1.45	-1.80	0.0378	0.0123
3	Pyruvate kinase isozymes M1/M2 - Homo sapiens	KPYM_HUMAN	340	8.99	53.498	3.15E-13	12	8	28	2.08	1.84	0.0425	0.1310
4	Alpha-enolase - Homo sapiens (Human)	ENOA_HUMAN	451	7.63	43.868	3.15E-24	12	12	36	-1.44	-1.04	0.0183	0.6037
5	Aspartate aminotransferase, mitochondrial precursor -	AATM_HUMAN	526	9.11	37.768	3.97E-22	11	17	24	3.55	2.20	0.0082	0.1506
6	Proto-oncogene C-crk - Homo sapiens (Human)	CRK_HUMAN	588	5.75	31.337	5.00E-05	4	25	15	-1.18	-1.57	0.1798	0.0304
7	dehydrogenase/cyclohydrolase, mitochondrial precursor	MTDC_HUMAN	599	7.62	30.741	1.99E-05	2	22	6	-1.52	-1.24	0.0378	0.0509
8	Nucleophosmin - Homo sapiens (Human)	NPM_HUMAN	617	5.28	28.629	9.98E-17	6	42	23	-1.45	-1.13	0.0063	0.1607
9	F-actin-capping protein subunit alpha-1 - Homo sapiens	CAZA1_HUMAN	624	5.82	28.077	5.00E-07	4	22	13	-1.31	-1.72	0.0848	0.0500
10	Protein S100-A6 - Homo sapiens (Human)	S10A6_HUMAN	627	5.53	27.715	6.29E-02	1	14	8	1.44	1.61	0.2047	0.0040
11	E3 ubiquitin-protein ligase BRE1A - Homo sapiens	BRE1A_HUMAN	690	7.24	24.011	1.99E+00	7	7	8	1.14	1.58	0.9413	0.0445
12	Cell division control protein 2 homolog - Homo sapiens	CDC2_HUMAN	716	8.41	22.598	7.92E-02	3	11	9	-1.24	-1.53	0.0589	0.0098
13	Proline synthetase co-transcribed bacterial homolog	PROSC_HUMAN	750	7.20	20.975	9.98E-09	5	15	20	1.16	1.52	0.9862	0.0135
14	Keratin, type I cytoskeletal 10 - Homo sapiens (Human)	K1C10_HUMAN	782	8.55	19.862	7.92E-19	16	36	27	-1.41	1.03	0.0380	0.0813
15	Triosephosphate isomerase - Homo sapiens (Human)	TPIS_HUMAN	830	6.50	18.830	2.51E-03	3	20	14	-1.45	-1.21	0.0477	0.0076
16	Histone deacetylase complex subunit SAP18 - Homo	SAP18_HUMAN	852	6.93	18.533	1.99E-01	4	5	33	1.48	1.24	0.0278	0.1628
17	Proteasome subunit beta type 1 precursor - Homo	PSB1_HUMAN	858	8.59	18.492	3.97E-10	7	19	42	-1.45	-1.14	0.0055	0.0939
18	Peroxiredoxin-1 - Homo sapiens (Human)	PRDX1_HUMAN	887	6.94	18.303	3.15E-02	2	15	10	1.58	1.41	0.0191	0.0778
19	Peroxiredoxin-1 - Homo sapiens (Human)	PRDX1_HUMAN	888	7.06	18.303	7.92E-20	7	14	37	1.37	1.52	0.0876[i]	0.1478[i]
20	Peptidyl-prolyl cis-trans isomerase B precursor - Homo	PPIB_HUMAN	988	9.14	18.488	2.51E-19	9	5	36	2.84	1.55	0.0163	0.2357
21	Cofilin-1 - Homo sapiens (Human)	COF1_HUMAN	1017	8.52	18.269	1.26E-05	9	38	49	-1.15	1.24	0.0757	0.0463
22	Nucleoside diphosphate kinase B - Homo sapiens	NDKB_HUMAN	1023	7.91	18.186	1.58E-09	4	16	31	-1.06	-1.56	0.3899	0.0214
23	Ubiquitin - Homo sapiens (Human)	UBIQ_HUMAN	1181	6.95	10.309	6.29E-06	4	13	49	1.60	1.29	0.0448	0.3933

Supplementary Table 1. Differential protein abundance of the 15 Min and 30 Min sample groups with respect to Control as determined from SyproRuby-stained gels. (a) Top hit from database (SwissProt) search. **(b)** The spots in Table 1 and 2 follow different numbering sequences. **(c)** pI and molecular weight are theoretical values for the identified protein. **(d)** from protein identification by mass spectrometry: the number of matches with equal or better scores that are expected to occur by chance alone. Note: We use the criterion E≤0.001 for the most reliable protein identification, however, other spots with E-values outside this limit are included for complete information when their SameSpots p values are ≤ 0.05. **(e)** number of peptides matched to the identified protein. **(f)** number of masses not matched to the identified protein. **(g)** percent of the protein sequence covered by the matched peptides. **(h)** from the pairwise comparison of

the treatment sample to the control sample; **(i)** three-group ANOVA (control-15 Min-30 Min) $p \leq 0.05$.

Supplementary Table 2

	Protein name[a]	Swissprot accession	Gel spot No[b].	pI[c]	MW (kD)[c]	MS ID Expectation value[d]	Peptide count[e]	Unmatched Masses[f]	Sequence coverage[g] (%)	Relative protein phosphorylation[h]		T-test p-value[h]	
										15 Min	30 Min	15 Min	30 Min
1	Endoplasmin precursor - Homo sapiens (Human)	ENPL_HUMAN	126	5.27	92.309	2.51E-79	30	35	38	1.16	-1.64	0.0001	0.6626
2	Elongation factor 2 - Homo sapiens (Human)	EF2_HUMAN	132	6.86	90.342	7.92E-40	23	36	28	1.62	1.04	0.0002	0.0050
3	L-lactate dehydrogenase B chain - Homo sapiens	LDHB_HUMAN	149	6.10	80.982	7.92E-07	7	50	25	1.29	1.00	0.0001	0.0592
4	FAST kinase domain-containing protein 5 - Homo	FAKD5_HUMAN	184	7.54	70.358	6.29E+00	7	15	9	-2.13	-1.96	0.0680[i]	0.2808[i]
5	ATP-dependent DNA helicase PIF1 - Homo sapiens	PIF1_HUMAN	213	9.09	64.324	1.58E+00	8	28	14	-1.43	1.43	0.0030	0.2294
6	Far upstream element-binding protein 1 - Homo sapiens	FUBP1_HUMAN	223	7.14	62.027	6.29E-45	18	23	29	2.79	1.50	0.1160	0.0315
7	Heterogeneous nuclear ribonucleoprotein L - Homo	HNRPL_HUMAN	248	7.12	55.230	1.99E-02	7	34	15	-1.22	1.89	0.0009	0.3617
8	ATP synthase subunit alpha, mitochondrial precursor -	ATPA_HUMAN	321	7.60	47.208	7.92E-39	20	21	47	1.33	1.20	0.0292	0.7893
9	Actin, cytoplasmic 2 - Homo sapiens (Human)	ACTG_HUMAN	419	6.06	37.978	3.97E-16	7	30	29	1.77	1.20	0.0861	0.0335
10	Heterogeneous nuclear ribonucleoprotein A1 - Homo	ROA1_HUMAN	539	9.19	26.159	9.98E-32	11	42	32	1.75	2.66	0.0492	0.2901
11	Myosin-Vc - Homo sapiens (Human)	MYO5C_HUMAN	555	6.88	24.295	2.51E+00	9	8	6	1.01	3.04	0.0318	0.8952
12	14-3-3 protein zeta/delta - Homo sapiens (Human)	1433Z_HUMAN	637	4.23	19.516	9.98E-18	9	12	37	1.08	1.13	0.0000	0.6583
13	Peroxiredoxin-1 - Homo sapiens (Human)	PRDX1_HUMAN	714	8.49	18.311	7.92E-37	9	30	42	-1.66	-1.18	0.0151	0.1740
14	Peroxiredoxin-1 - Homo sapiens (Human)	PRDX1_HUMAN	720	8.10	18.295	1.58E-28	11	34	44	-1.14	-1.08	0.0000	0.5392
15	Translationally-controlled tumor protein - Homo sapiens	TCTP_HUMAN	733	5.24	18.252	1.99E-10	5	17	28	-1.88	-1.36	0.5920	0.0035
16	COP9 signalosome complex subunit 8 - Homo sapiens	CSN8_HUMAN	758	5.77	18.342	6.29E-10	5	29	36	-1.60	1.95	0.0001	0.0044
17	Protein S100-A6 - Homo sapiens (Human)	S10A6_HUMAN	762	5.55	18.368	3.97E-03	2	12	16	-1.23	-1.71	0.0005	0.3527
18	NEDD8-conjugating enzyme Ubc12 - Homo sapiens	UBC12_HUMAN	770	8.18	18.433	1.58E-04	4	9	21	-1.11	-1.07	0.0113	0.5816
19	Dynamin-2 - Homo sapiens (Human)	DYN2_HUMAN	773	7.21	18.456	1.58E+00	9	29	15	-1.13	-1.17	0.0170	0.5289
20	Ubiquitin-conjugating enzyme E2 C - Homo sapiens	UBE2C_HUMAN	782	7.02	18.496	1.58E-02	5	34	31	1.05	1.37	0.0002	0.8644
21	Myosin regulatory light chain 2, nonsarcomeric - Homo	MLRM_HUMAN	809	5.08	18.306	7.92E-08	3	11	18	1.38	-1.21	0.0011	0.3279
22	40S ribosomal protein S19 - Homo sapiens (Human)	RS19_HUMAN	858	5.39	15.900	3.15E-02	1	21	6	-1.14	1.66	0.0001	0.5990
23	Ubiquitin-conjugating enzyme E2 N - Homo sapiens	UBE2N_HUMAN	859	6.28	15.900	3.97E-21	5	33	34	1.03	-2.09	0.0000	0.8836
24	Coactosin-like protein - Homo sapiens (Human)	COTL1_HUMAN	870	5.74	14.866	3.15E-28	6	15	31	1.55	1.02	0.0000	0.0069
25	Phosducin-like protein - Homo sapiens (Human)	PHLP_HUMAN	893	5.38	13.255	9.98E-01	6	26	26	1.53	1.80	0.1359[i]	0.4138[i]
26	Kidney-associated antigen 1 - Homo sapiens (Human)	KAAG1_HUMAN	908	8.63	12.000	2.51E+00	2	13	45	-1.86	-1.01	0.0000	0.0120
27	Keratin, type I cytoskeletal 14 - Homo sapiens (Human)	K1C14_HUMAN	909	4.97	11.945	1.58E-01	5	19	13	1.55	1.47	0.0000	0.0084
28	Bcl-2-related protein A1 - Homo sapiens (Human)	B2LA1_HUMAN	910	7.76	11.945	3.15E-01	5	21	34	-1.05	1.06	0.0000	0.6383
29	Thioredoxin - Homo sapiens (Human)	THIO_HUMAN	915	5.36	11.455	1.58E-20	4	19	42	1.37	1.53	0.0012	0.4464
30	Receptor-interacting serine/threonine-protein kinase 4 -	RIPK4_HUMAN	920	5.24	11.018	1.58E-01	5	5	6	1.68	1.59	0.0680[i]	0.3269[i]
31	Small nuclear ribonucleoprotein F - Homo sapiens	RUXF_HUMAN	925	5.14	10.582	7.92E-01	3	10	24	1.75	1.70	0.0593[i]	0.3720[i]
32	Copine-1 - Homo sapiens (Human)	CPNE1_HUMAN	1008	6.10	49.682	3.97E-08	6	46	12	-1.06	-1.72	0.0006	0.7524
33	Serine/threonine-protein kinase PAK 1 - Homo sapiens	PAK1_HUMAN	1020	6.67	18.300	3.15E-01	7	37	14	1.57	1.47	0.0001	0.0061
34	Vacuolar protein sorting-associated protein 29 - Homo	VPS29_HUMAN	1031	6.99	18.266	2.51E-02	2	8	14	-1.05	-1.13	0.0002	0.9573
35	60S acidic ribosomal protein P2 - Homo sapiens	RLA2_HUMAN	1045	4.79	14.932	1.58E-23	6	39	79	-1.04	-1.65	0.0000	0.7948
36	Myosin light polypeptide 6 - Homo sapiens (Human)	MYL6_HUMAN	1046	4.84	14.998	1.58E-23	2	46	11	-1.05	-1.33	0.0000	0.6282

Supplementary Table 2. Differential protein phosphorylation of the 15 Min and 30 Min sample groups with respect to Control as determined from Pro-Q Diamond-stained gels. (a) Top hit from database (SwissProt) search. **(b)** The spots in Table 1 and 2 follow different numbering sequences. **(c)** pI and molecular weight are theoretical

values for the identified protein. **([d])** from protein identification by mass spectrometry: the number of matches with equal or better scores that are expected to occur by chance alone. Note: We use the criterion E≤0.001 for the most reliable protein identification, however, other spots with E-values outside this limit are included for complete information when their SameSpots p values are ≤ 0.05. **([e])** number of peptides matched to the identified protein. **([f])** number of masses not matched to the identified protein. **([g])** percent of the protein sequence covered by the matched peptides. **([h])** from the pairwise comparison of the treatment sample to the control sample; **([i])** three-group ANOVA (control-15 Min-30 Min) p ≤ 0.05.

Supplementary Methods

Reagents

Noradrenaline, propranolol (non-specific ADRB blocker), xamoterol (ADRB1 agonist), terbutaline (ADRB2 agonist), butoxamine (ADRB2 inhibitor), isoproterenol (ADRB agonist), dibutyryl-cAMP (PKA agonist), ATP and hexamethonium bromide (peripheral ganglionic blocker; used at 1mg/kg; does not cross brain/blood barrier) were purchased from Sigma Aldrich (St. Louis, MO). Forskolin (cAMP agonist), H89, and KT5720 (PKA inhibitors) were purchased from Calbiochem (San Diego, CA). Recombinant PDGF and antibody against human $pSrc^{Y419}$ was purchased from R&D Biosystems (Minneapolis, MN). AP23846 (Src inhibitor) was obtained from ARIAD Pharmaceuticals. Antibodies against Src, $pSrc^{Y530}$, $pSrc^{Y416}$, and phospho-PKA substrates were purchased from Cell Signaling (Danvers, MA).

Cell Culture

The derivation and source of the established ovarian cancer cell lines HeyA8, SKOV3ip1, PC3, C8161, MB-231, and A2780-PAR have been reported previously [4,35,36]. Cells were maintained in RPMI 1640 supplemented with 15% fetal bovine serum and 0.1% gentamicin sulfate (Gemini Bioproducts; Calabasas, CA). SYF cells were purchased from the American Type Culture Collection (Manassas, VA) and maintained in Dulbecco's modified Eagle medium supplemented with 10% fetal bovine serum. All cell lines were routinely screened for Mycoplasma species (Fisher; Itasca, IL). All experiments were performed with cell cultures at 70%-80% confluence.

Protein Identification and Analysis

Matrix-Assisted Laser Desorption Ionization Time-of-Flight Mass Spectrometry (MALDI TOF/TOF MS) was used to analyze the samples and determine protein identification. MS and MS/MS spectral data were acquired with an Applied Biosystems 4800 MALDI TOF/TOF Proteomics Analyzer. Applied Biosystems software package included 4000 Series Explorer (v. 3.6 RC1) software with Oracle Database Schema Version (v. 3.19.0), Data Version (3.80.0) to acquire both MS and MS/MS spectral data. The instrument was operated in positive ion reflectron mode, mass range was 850 – 3000 Da, and the focus mass was set at 1700 Da. For MS data, 2000-4000 laser shots were acquired and averaged from each sample spot. Automatic external calibration was performed using a peptide mixture with reference masses 904.468, 1296.685, 1570.677, and 2465.199. Following MALDI MS analysis, MALDI MS/MS was performed on several (5-10) abundant ions from each sample spot. A 1kV positive ion MS/MS method was used to acquire data under post-source decay (PSD) conditions. The instrument precursor selection window was +/- 3 Da. For MS/MS data, 2000 laser shots were acquired and averaged from each sample spot. Automatic external calibration was performed using reference fragment masses 175.120, 480.257, 684.347, 1056.475, and 1441.635 (from precursor mass 1570.700). Applied Biosystems GPS Explorer™ (v. 3.6) software was used in conjunction with MASCOT to search the respective protein database using both MS and MS/MS spectral data for protein identification. Protein match probabilities were determined using expectation values and/or MASCOT protein scores. MS peak filtering included the following parameters: mass range 800 Da to 4000 Da, minimum S/N filter = 10, mass exclusion list tolerance = 0.5 Da, and mass

exclusion list (for some trypsin and keratin-containing compounds) included masses 842.51, 870.45, 1045.56, 1179.60, 1277.71, 1475.79, and 2211.1. For MS/MS peak filtering, the minimum S/N filter = 10.

For protein identification, the *Homo sapiens* taxonomy was searched in the SwissProtein database. Other parameters included the following: selecting the enzyme as trypsin; maximum missed cleavages = 1; fixed modifications included carbamidomethyl (C) for 2-D gel analyses only; variable modifications included oxidation (M); precursor tolerance was set at 0.2 Da; MS/MS fragment tolerance was set at 0.3 Da; mass = monoisotopic; and peptide charges were only considered as +1. The significance of a protein match, based on both the peptide mass fingerprint (PMF) in the first MS and the MS/MS data from several precursor ions, is based on expectation values; each protein match is accompanied by an expectation value. The expectation value is the number of matches with equal or better scores that are expected to occur by chance alone. The default significance threshold is $p<0.05$, so an expectation value of 0.05 is considered to be on this threshold. We used a more stringent threshold of 10^{-3} for protein identification; the lower the expectation value, the more significant the score.

Microarray Analysis

cDNA microarray was performed using the Affymetrix platform on SKOV3ip1 cells that were treated with NA. After, NE treatment, mRNA was extracted and its purity and integrity assessed by utilizing an Agilent 2100 bioanalyzer (Agilent Technologies, Santa Clara, CA). Genome-wide transcription profiling was carried out using Affymetrix U133A high-density oligonucleotide arrays (Affymetrix, Santa Clara, CA) in the UCLA DNA

Microarray Core, as previously described (Cole, et al. 2009). Low level gene expression was quantified by Robust Multiarray Averaging and differentially expressed genes were identified by a ≥ 2-fold difference in mean expression level (corresponding to a 5% False Discovery Rate). Gene expression data are deposited in the National Center for Biotechnology Information Gene Expression Omnibus under the accession number GSE34405.

Plasmids and Transfections

The wild-type (WT) Src and S17A Src plasmids were a kind gift from Philip J. Stork (The Vollum Institute, Portland, OR). Lipofectamine 2000-mediated transfections were carried out according to instructions provided by the manufacturer (Invitrogen, Carlsbad, CA). Following transfection, the SYF cells were allowed to recover in medium for 24 h. Cells were then starved overnight in serum-free Dulbecco's modified Eagle medium before treatment.

Generation of A2780-ADRB2 cells

The cDNA of ADBR2 was extracted from a pCDNA 3.1 plasmid containing its sequence (Missouri S&T cDNA Resource Center; Rolla, MO). Following digestion by XbaI and BamH1 the ADRB2 sequence was cloned into an OG2 expression vector through the same two restriction enzyme sites. The inserted ADRB2 sequence was confirmed by sequencing. The lentivirus was then produced by transfecting human embryonic kidney cells (293FT; Invitrogen, Carlsbad, CA) with the sequence-verified OG2 vector containing either the ADBR2 or an empty vector, the packaging plasmid (MD2G), and

the envelope plasmid (PAX2), which are required for viral production. Three days later, the viral supernatant was collected and filtered to remove cellular debris. A2780-PAR cells were plated at 70% confluence in 6-well plates and transduced with the virus. After 16 h, the virus-containing medium was removed and replaced with normal growth medium. Transduced cells were selected by resistance to puromycin.

Intraovarian Orthotopic Implantation of Tumour cells

For metastasis-specific *in vivo* models, SKOV3ip1 (1.6×10^6) cells were suspended in 30 µl of Hanks' balanced salt solution (Invitrogen) and injected directly into the right ovary of anesthetized nude mice through a 1.5-cm intraperitoneal incision. One week after cell injection, staples were removed, and mice were subjected to daily restraint stress. Control siRNA or Src siRNA-DOPC treatment was also started 7 days after tumour cell injection. Following tumour cell injection, restraint stress was continued for an additional 3 weeks. Src and Control siRNA-DOPC therapy was continued twice weekly until the end of the experiment. At this point, mice were sacrificed; tumours were harvested, and the tumour weight and number and location of nodules were recorded.

Src Immunoprecipitation

Src precipitation was performed by incubating 100 µg of whole cell lysate with a Src antibody overnight at 4ºC. Protein-antibody complexes were incubated for 2 h with protein A agarose–conjugated beads, collected by centrifugation, washed three times with modified radioimmunoprecipitation assay buffer, and boiled in Laemmli sample

buffer. The proteins were separated by SDS-PAGE and immunoblotted as described in the Western blot analysis section.

Kinase Assay

For kinase assay shown in Supplementary Figures 2 and 4g, HEK 293 cells transiently expressing Flag-tagged FAK, Flag-tagged kinase-dead FAK or Flag-tagged Src were individually lysed and protein concentration for each sample was determined. For kinase assay shown in Supplementary Figure 4i, SKOV3ip1 cells were lysed and its protein concentration was determined. 300 µg of each cell lysate were combined. Samples were incubated overnight with a Flag, Src or FAK antibody. Protein-antibody complexes were precipitated for 1 hour using agarose-conjugated mouse secondary antibody. Immune complexes were washed three times with RIPA buffer, one time with Tris pH 7 and one time with kinase buffer with no ATP. The kinase reaction was carried out by adding 25 µL of kinase buffer containing ATP or an ATP/pS17 peptide and incubating for 30 minutes. The reaction was stopped by adding 25 µL of Laemmli sample buffer and boiling samples. Afterwards, samples were subjected to Western blot analysis. For kinase assay shown in Supplementary Figure 4h, ADP-Glo Src kinase assay kit was used following the manufacturer's protocol (Promega, Madison, WI).

Immunofluorescence analysis for pSrc^{Y419}

SKOV3ip1 and HeyA8 cells were incubated on chamber slides and serum starved overnight, exposed to NE for 10 min, fixed in 4% formaldehyde, permeablized in cold methanol, incubated overnight with an actin antibody (Cell Signaling, Danvers, MA),

visualized with an anti-rabbit secondary antibody conjugated to an Alexa 488 fluorochrome (Molecular Probes, Eugene, OR), and an pSrcY419 linked to an Alexa 555 fluorochrome (Millipore, Temecula, CA) was subsequently added for 2 hrs. Slides were then washed, coverslipped and visualized.

Immunohistochemical Analysis for Src and pSrc^{Y419}

Following approval by the Institutional Review Board, 91 ovarian cancer samples from M. D. Anderson Cancer Center and the University of Iowa Hospital and Clinics were obtained. These formalin-fixed, paraffin-embedded human samples were stained for total Src and pSrc^{Y419}. Slides were heated overnight at 65ºC and then dewaxed using graded xylenes. Antigen retrieval was performed using Borg Decloaking solution using a vegetable steamer for 40 min and followed by a 30-min cool-down. Endogenous peroxidase activity was blocked by incubation in 3% hydrogen peroxide (in methanol) for 12 min. The protein blocking solution was applied for 30 min using an Fc Receptor Blocker (Innovex Biosciences, Richmond, CA). Primary antibodies were applied at a dilution of 1:300 and incubated overnight in a humidity chamber at 4ºC. Secondary antibodies were visualized using the MACH4+ polymer-linked horseradish peroxidase system (Biocare, Concord, CA). 3,3'-Diaminobenzidine was applied, and staining was monitored visually under a bright field microscope (~ 3-4 min). Counterstaining was performed using Gill's Hematoxylin for 10 sec, followed by washing with phosphate-buffered saline. Slides were dried and mounted using universal mounting medium and then scored by a board-certified pathologist. Src or pSrc^{Y419} expression was determined by assessing semi-quantitatively the percentage of stained tumour cells and the staining

intensity, as described previously (Sood, AK, et al. 2004). Briefly, the percentage of positive cells and staining intensity were rated on a scale of 1 to 4; points for expression and percentage of positive cells were added, and an overall score (OS) was assigned. Tumours with an OS in the upper tertile were considered as having protein overexpression. The stained slides were also scored on the basis of the histochemical score (with a score > 100 defined as high expression and ≤ 100 as low expression), according to the method described by McCarty et al., which considers both the intensity of staining and the percentage of cells stained (McCarty KS, et al. 1985; Singh M, et al. 2007; Merritt WM, et al. 2008). An ovarian cancer tissue lacking the primary antibody was used as a negative control.

Noradrenaline concentration

Pre-surgical blood samples were collected between 6:30 and 11:30 AM (average 8:20 AM, an average 3 hrs before tumour tissue capture), drawn into chilled EDTA Vacutainers (BD Biosciences, Franklin Lakes, NJ), and maintained on ice prior to centrifugation, separation of the plasma, and storage at -80°C until the time of extraction and assay. Plasma catecholamines were absorbed onto activated alumina at pH 8.6, washed, and eluted with dilute acid prior to injection onto a reverse-phase column to separate the individual catecholamines. Detection was accomplished by the use of a Coulochem II Dual Potentiostat Electrochemical Detector (ESA, Chelmsford, MA.). A calibration curve using “blank” human plasma (dialyzed to remove endogenous catecholamines) and linear regression analysis was used to determine sample plasma noradrenaline concentration. The calibration curve used the internal standard (DHBA,

3,4 dihyroxybenylamine) method which calculates an average response factor using peak areas and concentrations of added catecholamine in relation to the peak area of the internal standard. The interassay and intra-assay coefficients of variation were 3.4 and 3.1%, respectively, and the lower limit of detection was 25 pg / ml.

Dissected 2-3 mm^3 tumour tissue samples were snap frozen in liquid nitrogen, pulverized using liquid nitrogen, and held on dry ice. The tissue powder was weighed and briefly homogenized (Fisher PowerGen 500 and sawtooth generator) in 5 ml 0.4 M perchloric acid containing 6 mM glutathione. Following centrifugation of the homogenate (1000 × g, 30 min), the supernatant was neutralized with 5 ml of TRIS buffer (1.5 M, pH 8.5) and catecholamines were absorbed onto acid washed alumina (100 mg). The alumina was washed twice with water and catecholamines were eluted with 1 ml 0.05 M perchloric acid containing 0.1 mM sodium metabisulfite. After microfiltration, the eluate was diluted in 4% acetic acid, and catecholamines were resolved using an Aquasil C18 4 µm (100 × 4.6 mm) HPLC column (Thermo Electron Corp., Bellefonte, PA), followed by electrochemical detection as described above. Chromatograph peak areas for noradrenaline and adrenaline were compared to the average peak areas determined from the injection of 100 pg pure standard, and corrected for extract dilutions and tissue wet weights.

Molecular Dynamic Simulation

The starting structures for the docking experiments were prepared with the leap module within the Assisted Model Building with Energy Refinement (AMBER) package, version

1.2 (54). These tools were used for adding the phosphate group to residue S17. The charges used for the unmodified amino acid were obtained from the amber99SB force field (ff99SB) (55), and the charges for the phosphorylated amino acid from H. Sticht et al (56). The structure and topology files for the peptide and the c-Src were converted to pdb files that resemble a pqr file using the ambpdb tool from the AMBER 10 package (57). The resulting pdb file was then processed with Autodock tools (58) to create the input for Autodock Vina (59). Six independent docking experiments were made. In four of them, the side chains and backbone were allowed to move, and in the remaining two, only the side chain and the terminal residues were allowed to move. From each experiment, one or two structures were taken, for a total of nine structures that were used as initial structures for molecular dynamics experiments.

All of the peptide/c-Src molecular dynamics simulations were carried out with the canonical ensemble using the SANDER module of the AMBER 10 package (60). Solvation effects were incorporated using the Generalized Born model (igb=5) (61), as implemented in AMBER. All hydrogen bonds were constrained using SHAKE (62), and a cutoff of 16 Å was used for long-range interactions, along with a base time step of 2 ps.

All simulations were energy minimized in 500 steps with a steep descent algorithm, followed by 500 steps of conjugate gradient minimization. During the 300 ps heating phase, the temperature was raised from 0 to 300 K, and positional restraints were applied to all atoms. After this, the constraints on the side chains were released,

constraining only the backbone of the protein and the peptide. After this phase, all constraints were removed and the simulations were at least 1 ns. After 1 ns, the simulations were analyzed periodically for any particular behavior. Only one of the simulations was selected for extended molecular dynamics simulations. The starting structure from this simulation was edited to create two other systems with the same starting configuration: one with c-Src and the unphosphorylated peptide and the other with c-Src alone. The simulations of the remaining three systems were extended for 30 ns.

Molecular Images

Molecular graphics images were produced using the University of California, San Francisco Chimera package from the Resource for Biocomputing, Visualization, and Informatics at the University of California, San Francisco (supported by NIH P41 RR-01081), VMD, and Pymol.

Statistical Analysis of the FDA's Adverse Event Reports

Collection and Preprocessing of AE Reports

Adverse event reports (annual quarter releases from 2004Q1 to 2009Q2) were obtained from the FDA's Adverse Events Reporting System (AERS) and were organized in the fashion described below. An adverse event (AE) in principle corresponds to a single patient and it may be described via different reports. In these reports the medications applied for the patient therapy (and partially indications) are listed, as well as outcomes and side effects of patients.

Using text mining methods, the free-text descriptions (descriptions in prose) of the medications involved in the reported patient treatments (no controlled vocabulary is imposed by the FDA) were mapped to entries from DrugBank 2.5 as far as this was possible. DrugBank drugs were further mapped to Anatomic Therapeutic Chemical (ATC, from WHO; version of 2009) Classification System terms whereas indications and reactions reported in AEs are encoded in MedDRA (for the analysis, MedDRA Version 2009 was used) terms.

Counting of relevant AEs

AEs related to cancer treatments were isolated. These were defined as those AEs for which either: (a) a reported indication was assigned to a cancer-related MedDRA term, or (b) any of the reported medications was mapped to a DrugBank record associated to ATC codes related to cancer treatment. This approach resulted in 262,262 cancer related AEs. Second, the list of beta-blocker drugs (BBs) was isolated from the ATC hierarchy; any cancer-related AE for which a patient case refers to any of these BBs was considered to have been treated with BBs. This approach resulted in 18,127 cancer AEs that were treated with BBs. Third, cancer-related AEs were distinguished between those reporting that the patient had died (by checking whether the term 'Death' was explicitly reported as outcome or as side effect). This approach yielded 2,777 cancer-related AEs treated with BBs and 43,662 cancer AEs not treated with BBs to have been fatal. Then, the subset of AEs for which cancer-related indications had been explicitly reported was sub-divided into ‘therapy-groups’ according to MedDRA hierarchical

categorization. For the different levels of the MedDRA ontology the AEs corresponding to each therapy-group term were divided in four groups: (a) those treated with BBs and the patient died (with $n_{dead,1}$ denoting their count); (b) those treated with BBs and the patient survived ($n_{sick,1}$); (c) those not treated with BBs and the patient died ($n_{dead,0}$); (d) those not treated with BBs and the patient survived ($n_{sick,0}$). Not all cancer-related MedDRA terms (from each level of the hierarchy, i.e., therapy-groups) were reported in AEs as indications, whereas for some of the remaining therapy-groups (i.e., associated to AEs) the number of AEs clustered around the respective terms has not been adequate to yield statistical significance.

Adverse Event Reporting Model

Next we sought to infer whether treatment with a beta blocker induced any change in patient mortality, given the specific cancer or cancer-related morbidity. To do so, we tried to estimate separately the mortality rates of patients who received BBs and of patients who did not. However, while these rates do influence the observed case counts, they can potentially be confounded by unobserved factors (e.g., the fraction of patients who submit a report) and can thus cannot be computed without additional data. However, on the basis of reasonable assumptions, it is possible to estimate the quotient of two such ratios. In order to detail this, we first introduced a formal notation.

In the following, we considered a fixed cancer type C; for simplicity this is not made explicit in the notation. We denoted by p_{sick} and p_{dead} and the probability that a C-patient experiences non-lethal or lethal adverse events, respectively. We assumed that only

part of them, say r_{sick}, $r_{dead} \leq 1$, submitted a report, such that the cases show up in our counts of reported AEs. Furthermore, our model can handle the case $r_{sick} \neq r_{dead}$, which is important, as it seems likely that $r_{dead} > r_{sick}$ holds in reality. It is reasonable to assume that event probabilities (p_{sick} and p_{dead}) depend on the treatment, including medication, while for the reporting rates (r_{dead}, r_{sick}) this seems less intuitive, such that we can treat them as constant. Our final assumption was that p_{sick} is not substantially changed for cancer patients by administering BBs. This may be justified due to the relatively minor side effects of BBs, as compared to those of anti-cancer drugs. Let b be the fraction of patients that receive any beta blocker.

The above modelling for N patients contracting C is formalized as:

$$n_{dead,1} = N * b * p_{dead}(BB=1) * r_{dead} \quad (S1)$$

$$n_{sick,1} = N * b * p_{sick} * r_{sick} \quad (S2)$$

$$n_{dead,0} = N * (1-b) * p_{dead}(BB=0) * r_{dead} \quad (S3)$$

$$n_{sick,0} = N * (1-b) * p_{sick} * r_{sick} \quad (S4)$$

Here $p_{dead}(BB=1)$ and $p_{dead}(BB=0)$ are the death rates that we would like to know and compare: the probability of dying from cancer C when receiving or not receiving BBs. In practice we start out by computing the two *reported death rates*: that for patients who received a beta blocker,

$$dr(BB=1) := n_{dead,1} / [n_{dead,1} + n_{sick,1}] = p_{dead}(BB=1) / [p_{dead}(BB=1) + p_{sick}] \quad (S5)$$

and the analoguously defined dr(BB=0), for the cases not treated with any beta blocker.

We now show that their quotient approximates the odds of the true death rates. For brevity we write p_{D1} for $p_{dead}(BB=1)$ and likewise p_{D0} for the mortality rate without beta

blockers.

$$dr(BB=1) / dr(BB=0) \qquad \text{(S6)}$$

$$= p_{dead}(BB=1) / [\, p_{dead}(BB=1) + p_{sick} \,] / \{\, p_{dead}(BB=0) / [\, p_{dead}(BB=0) + p_{sick} \,] \,\} \qquad \text{(S7)}$$

$$= p_{D1} \,(\, p_{D0} + p_{sick} \,) / \{\, p_{D0} \,(\, p_{D1} + p_{sick} \,) \,\} \qquad \text{(S8)}$$

$$= \{\, p_{D1}\, p_{D0} + p_{D1}\, p_{sick} \,\} / \{\, p_{D1}\, p_{D0} + p_{D0}\, p_{sick} \,\} \qquad \text{(S9)}$$

$$\approx \{\, p_{D1}\, s \,\} / \{\, p_{D0}\, s \,\} \qquad \text{(S10)}$$

$$= p_{dead}(BB=1) / p_{dead}(BB=0) \qquad \text{(S11)}$$

The approximation in the second but last line holds, since the death rates p_{D0} and p_{D1} can be assumed to be substantially smaller than the complication rate p_{sick}. Further, as $(a+c)/(b+c) \to 1$ for $c \to \infty$, our estimates of death rate odds are conservative. Finally, we report 1 - dr(BB=1) / dr(BB=0) as the relative decrease of mortality.

Bayesian Inference

In the above model, we have simplistically assumed that the numbers of reported cases are directly proportional to the underlying probabilities. The corresponding estimates of ratios by quotients of case numbers are hence called naive. In order to obtain more realistic estimates, we applied Bayesian inference. Specifically, we use a two-level hierarchical prior; the first level is on the reported death rate of a cancer C in general (without beta blocker treatment), the second prior is on the corresponding rate with beta-blockers. The arrangement is hierarchical in terms of information flow: The second prior is parameterized to match the expectation value of the posterior without BB. The

top-level prior is set up to match the overall reported death rate as naively estimated from the entire large body of data on all cancer types. For both levels of priors we used beta distributions, as they are conjugated to the binomial distribution, and tuned them to match 10 pseudo-observations.

After computing the posterior beta distributions over the reported death rate with and without beta blocker, we determine their expectations and form their quotient as estimate of dr(BB=1) / dr(BB=0). In addition, we infer the posterior distribution of this quotient and numerically integrate to obtain the probability of it being smaller than one. This probability directly yields a measure of confidence in the observed mortality reduction.

Supplementary References

54. Zhang W, Hou T, Schafmeister C, Ross WS, and DA Case (2008). The leap module of AMBER tools 1.2. University of California, San Francisco.
55. Hornak V, Abel R, Okur A, Strockbine B, Roitberg A and C Simmerling. PROTEINS: Structure, Function, and Bioinformatics 65:712–725 (2006).
56. Homeyer N, Horn AHC, Lanig L, H Sticht. AMBER force field parameters for phosphorylated amino acids in different protonation states: phosphoserine, phosphothreonine, phosphotyrosine and phosphohistidine J. Mol. Model. 2006, 12, 281-289.
57. Case DA, Darden TA, Cheatham TE, Simmerling CL, Wang J, Duke RE, Luo R, Crowley M, Walker RC, Zhang W, Merz KM, Wang B, Hayik S, Roitberg A, Seabra G, Kolossváry I, Wong KF, Paesani F, Vanicek J, Wu X, Brozell SR, Steinbrecher T, Gohlke H, Yang L, Tan C, Mongan J, Hornak V, Cui G, Mathews DH, Seetin MG, Sagui C, Babin V, and PA Kollman (2008), AMBER 10, University of California, San Francisco.
58. Sanner MF. Python: A Programming Language for Software Integration and Development. J. Mol. Graphics Mod., 1999, Vol 17, February. p57-61.
59. Trott O and AJ Olson. AutoDock Vina: improving the speed and accuracy of docking with a new scoring function, efficient optimization and multithreading, Journal of Computational Chemistry 31 (2010) 455-461.
60. Case DA, Darden TA, Cheatham TE, Simmerling CL, Wang J, Duke RE, Luo R, Crowley M, Walker RC, Zhang W, Merz KM, Wang B, Hayik S, Roitberg A, Seabra G, Kolossváry I, Wong KF, Paesani F, Vanicek J, Wu X, Brozell SR,

Steinbrecher T, Gohlke H, Yang L, Tan C, Mongan J, Hornak V, Cui G, Mathews DH, Seetin MG, Sagui C, Babin V, and PA Kollman (2008), AMBER 10, University of California, San Francisco.

61. Onufriev A, Bashford D, Case DA. Exploring protein native states and large-scale conformational changes with a modified generalized Born model. Proteins, 2004, 55,383–394.
62. Ryckaert JP, Ciccotti G, Berendsen HJC. Numerical integration of the cartesian equations of motion of a system with constraints: Molecular dynamics of n-alkanes. J. Comput. Phys., 1977, 23, 327–341.
63. We have deposited the cDNA microarray data into the NCBI GEO database under accession number GSE34405.